THE JOURNAL OF PHYSICAL CHEMISTRY B

Article

Cite This: J. Phys. Chem. B 2017, 121, 10371-10381

pubs.acs.org/JPCB

Freezing Temperatures, Ice Nanotubes Structures, and Proton Ordering of TIP4P/ICE Water inside Single Wall Carbon Nanotubes

P. Pugliese, M. M. Conde, M. Rovere, and P. Gallo*

Dipartimento di Matematica e Fisica, Università Roma Tre, Via della Vasca Navale 84, 00146 Roma, Italy

ABSTRACT: A very recent experimental paper importantly and unexpectedly showed that water in carbon nanotubes is already in the solid ordered phase at the temperature where bulk water boils. The water models used so far in literature for molecular dynamics simulations in carbon nanotubes show freezing temperatures lower than the experiments. We present here results from molecular dynamics simulations of water inside single walled carbon nanotubes using an extremely realistic model for both liquid and icy water, the TIP4P/ICE. The water behavior inside nanotubes of different diameters has been studied upon cooling along the isobars at ambient pressure starting from temperatures where water is in a liquid state. We studied the liquid/solid transition, and we observed freezing temperatures higher than in bulk water and that depend on the diameter of the nanotube. The maximum freezing temperature found is 390 K, which is in remarkable agreement with the recent experimental measurements. We have also analyzed the ice structure called "ice nanotube" that water forms inside the single walled carbon nanotubes when it freezes. The ice forms observed are in agreement with previous results obtained with different water models. A novel finding, a partial proton ordering, is evidenced in our ice nanotubes at finite temperature.

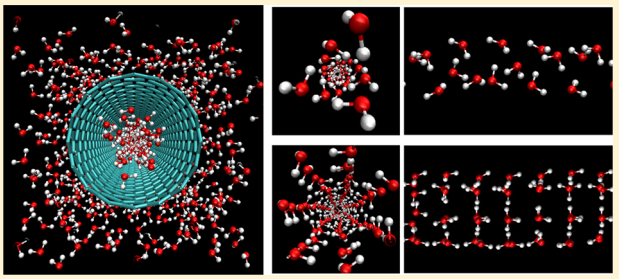

INTRODUCTION

Water is the most important molecule present on our planet. It plays a fundamental role in both geological and chemical processes,[1] and it is also essential for life.[2] The study of confined water in particular is an issue of wide interest as it not only allows us to investigate the general properties of water[3,4] but also has applicative purposes.[5]

Among confining structures carbon nanotubes (CNTs) have attracted in recent times a great interest due to their fascinating properties that made them potentially useful in a wide variety of applications. These cylindrical nanostructures are formed by one or more layers of graphene. Among the numerous applications[6] there are the use of CNTs in electronic devices[7] and their usage in biology and medicine.[8,9] A considerable number of applications are connected to water: for example, the study of the water flow through atomic smooth surface of a carbon nanotubes[10] and its enhancement found by both theoretical calculations[11] and experiments,[12] or the study of membranes made by carbon nanotubes that can be also used as filter in desalination mechanisms for different solutions like the NaCl aqueous solution.[13,14]

Water can fill the space inside a single walled carbon nanotube (SWCNT),[15,16] and it was found both experimentally[17−19] and by simulation[20,21] that it easily crystallizes. The water ordered structures that form inside the SWCNTs are called ice nanotubes[22] and consist of a series of stacked ordered polygonal rings of water molecules. The number of water molecules in the ring depends on the size of the nanotube. And for the smallest diameters the rings form a spiral stack.[22]

Importantly and unexpectedly it was recently experimentally discovered by an MIT group[23] that water freezes already at boiling conditions inside the nanotube. Thus, the hydrated SWCNTs can be considered as possible candidates for the latent thermal storage in diverse systems.[24]

Molecular dynamics simulations on water in carbon nanotubes focusing on solid/liquid transition[20,22] have used a model, TIP4P, that has a freezing temperature in the bulk phase 42.65 K lower than experimental bulk water at ambient pressure.[25] This inevitably leads also to a downward displacement of the freezing temperatures inside the carbon nanotubes.

Due to the large interest in this issue and to the importance of molecular dynamics simulations as complement to experimental findings, it is timely to use better potentials for the simulation studies.

In this work we perform molecular dynamics simulations for the water molecules using a very realistic potential: the TIP4P/ICE.[26] This model was designed to study the solid phases of water and gives also the best overall ice phase diagram and the best predictions for the densities of several ice forms. In the past years, this model has been successfully used in the study of different ice systems[27−33] and clathrate systems.[34−37]

We study here with this potential the liquid/solid transition temperatures and we compare them to the recent experimental findings of ref 23. We also analyze the kind of ordered structures that form by varying the diameter of the SWCNT focusing also on the positions of the hydrogens.

The paper is organized as follows: in the next section the methods and materials are described. The third section shows

Received: June 28, 2017
Revised: October 17, 2017
Published: October 17, 2017

DOI: 10.1021/acs.jpcb.7b06306
J. Phys. Chem. B 2017, 121, 10371−10381

the process of water crystallization inside the SWCNT. In the fourth section we study in detail the ordering of the water structures inside the SWCNT. Finally, the main conclusions are discussed.

METHODS AND MATERIALS

The SWCNT can be conceptualized as a slice of graphene wrap forming a seamless cylinder. Each nanotube can be identified by the way in which the graphene sheet is cut before wrapping. This way is represented by a pair of indices (n,m). The integers n and m denote the linear combination of unit vectors along which the slice of graphene is cut. In our work we used a particular choice for the two indices, with $m = 0$ that produces what is called a zigzag SWCNT. The diameter of the nanotube for this configuration is given by the value of n through the relation

$$d = \frac{\sqrt{3}}{\pi} an \tag{1}$$

where $a = 0.142$ nm is the value for the lattice space between the carbon atoms (the length of the side of the hexagon).[38,39] This equation implies that we cannot change continuously the diameter of the SWCNT in order to produce a completely ordered structure.

After the sheet was wrapped we saturated the carbon dangling bonds at the two extremes of the nanotube with hydrogens as common practice. Graphene is a very stable material and interacts very weakly with external molecules. For this reason we choose, as also done in literature,[22] to reproduce the interactions of the SWCNT and the water molecules as a Lennard-Jones potential:

$$V(r) = 4\varepsilon\left[\left(\frac{\sigma}{r}\right)^{12} - \left(\frac{\sigma}{r}\right)^{6}\right] \tag{2}$$

We used the OPLS all atom potential parameters[40] to simulate the SWCNT. The SWCNT lattice was kept rigid. The nanotube was inserted in a water box so that the SWCNT was completely surrounded and filled by water molecules. The water molecules in our system are described by the TIP4P/ICE potential.[26] This is a rigid planar model that consists of a Lennard-Jones site for the oxygen atom, and three charged sites. The positive charges are located on the two hydrogens, and the negative charge is located on a virtual site M situated at distance OM = 0.01577 nm from the oxygen along the H−O−H bisector.

The Lennard-Jones potential parameters (see eq 2) that we have used in our simulations, for both water and SWCNT, are reported in Table 1. The cross-interaction parameters are calculated with the Lorentz−Berthelot mixing rules.

We have studied water inside SWCNT for different sizes of the nanotubes. In Table 2 we report the characteristics of the different systems that we have studied as the diameter (d) and length (L) of the SWCNT, the number of water molecules N_W, and the size of the initial simulation box. The axis of the cylinder was oriented in our simulation parallel to the y axis. In all the cases the length of the SWCNT is much longer than the diameter.

Table 1. Lennard-Jones Parameters and Value of the Charges of the SWCNT and the TIP4P/ICE

	atom	σ [nm]	ϵ [kcal/mol]	q[e]
SWCNT	C	0.355	0.29288	
	H_C	0.242	0.12552	
water	O	0.31668	0.88218	
	H_W			0.5897
	M			−1.1794

Table 2. Geometrical Specifications of the Different Simulated Systems[a]

d [nm]	L [nm]	n	N_W	N_C	x [nm]	y [nm]	z [nm]
0.978	19.246	13	1884	2340	2.018	23.282	2.018
1.056	19.246	14	2624	2520	2.096	23.438	2.096
1.213	19.246	16	2979	2880	2.252	23.750	2.252
1.291	19.246	17	3213	3060	2.330	23.906	2.326
1.369	19.246	18	3469	3240	2.410	24.066	2.410

[a] d is the diameter of the nanotubes, L is the length of the nanotube, n is the structure index, N_W is the number of water molecules contained in the simulation box, N_C is the number of carbon atoms that form the SWCNT, and x, y, and z are the lengths of the simulation boxes for the highest temperature investigated.

We performed the simulations using the software GROMACS (version 5.0.7).[41] The simulation box size was changed depending on the nanotube diameter in order to have the smallest box that still allows the water molecules to surround the SWCNT. Periodic boundary conditions along all three axes were applied in all simulations. An example of a simulation box is reported in Figure 1 for the system with a diameter of $d = 1.213$ nm.

We performed our simulations in the isothermal−isobaric ensemble (NpT). For each diameter chosen for the SWCNT we started from a high temperature where water is liquid inside the SWCNT. The starting temperatures for each system are reported in Table 3. We cooled each system along the $p = 1$ bar isobar. For each temperature we reach equilibrium using the Berendsen thermostat. For the pressure control we use the Parrinello−Rahman barostat. Since the simulations of such a large system are rather time-consuming, we used the shifted force method with a cutoff at 0.9 nm for all interactions. Particle-mesh Ewald (PME) was used to determine the long-range forces in the systems.

We performed MD simulations of five pores with different diameters. For each pore we simulated from 20 to 36 different temperatures. Starting from the temperatures T_{max} reported in Table 3, we cooled each system with step of 10 K simulating a total of 130 state points for this study.

The typical time required for the dipolar reorientation of water molecules inside SWCNT has been reported to be on the order of 0.7 ps.[42] For this reason we choose a time step of 0.001 ps for our simulations. The length of each simulation run is 5 ns.

RESULTS

Crystallization of Water inside the SWCNT. Our work focuses on the cooling processes of the water inside SWCNTs and the icy structures that form inside the nanotubes. We consider indeed for the analysis of results only the water molecules present inside the SWCNT.

In order to find the temperature of crystallization of the water inside the SWCNT, we analyze both the trend of the potential energy and the radial distribution functions of the inner water molecules. To calculate the potential energy, we used the GROMACS tool "gmx energy" considering only the

DOI: 10.1021/acs.jpcb.7b06306
J. Phys. Chem. B 2017, 121, 10371−10381

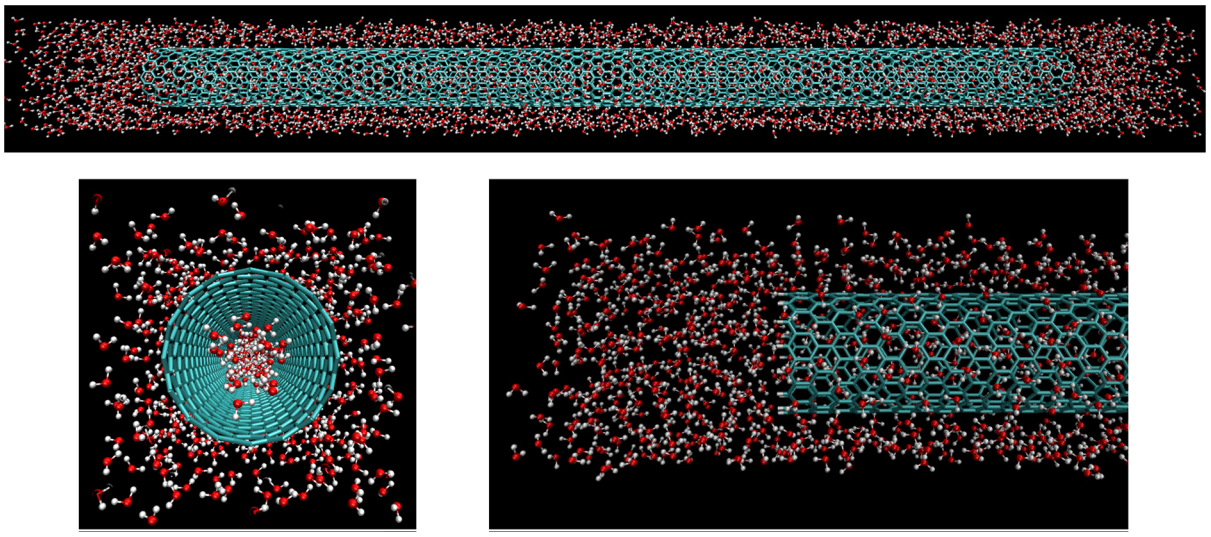

Figure 1. Snapshots of the system with a SWCNT of diameter d = 1.213 nm (n = 16) for the equilibrated sample at the highest temperature investigated, T = 450 K. The three snapshots represent respectively the side view of the whole simulation box (top figure), a cut and blowup of the frontal view (bottom left figure), and a cut and blowup of the side view (bottom right figure).

Table 3. Maximum (T_{max}) and the Minimal (T_{min}) Temperatures from Which Each System Is Cooled along the p = 1 Bar Isobar

d [nm]	T_{max} [K]	T_{min} [K]
0.978	350	150
1.056	500	150
1.213	450	150
1.291	350	150
1.369	350	150

water−water interaction of the water molecules inside the SWCNT.

In Figure 2 we can see the behavior of the potential energy of the water molecules that are inside the SWCNT at different temperatures. It is interesting to note that for the four larger nanotubes the curves at low temperatures collapse on the same line, while the curve of the potential energy of water inside the smallest SWCNT is quite different. This behavior is most likely due to the difference in the structure of the ice that forms inside the smallest SWCNT. We will in fact see in the next subsection and in Figure 7 that all ice nanotubes investigated are formed by stacked rings except the smallest one that is formed by spiraling rings. We will better discuss the details of the structure later in the next subsection.

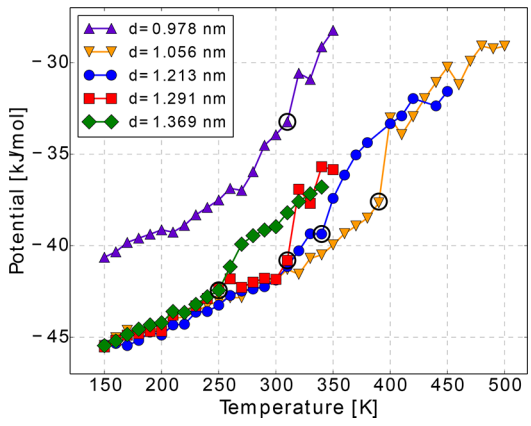

Figure 2. Potential energy of the water molecules that fill the SWCNTs as a function of the temperature T. The different curves are relative to the different diameters of the nanotube as reported in the legend. The black empty circle marks the freezing temperature.

We identify the temperature where water freezes inside the SWCNTs, T_F, as the temperature where the potential energy shows an abrupt decrease.

To confirm the results obtained for the potential energy, we have studied also the behavior of the radial distribution functions of our systems. In Figure 3 we report as an example the $g(r)$ for oxygen−oxygen, oxygen−hydrogen, and hydrogen−hydrogen relative to the inner water of the nanotube with a diameter of d = 1.291 nm (n = 17) at the different temperatures investigated.

The $g(r)$ values obtained by a molecular dynamic simulation in a confined system are generally different from the ones obtained in bulk water. In order to normalize the $g(r)$ in the correct way,[43,44] it is necessary apply a form factor due to the geometry of the confinement so that the $g(r)$ goes to 1 at infinite distance. In Figure 3 and in the following figures showing the radial distribution functions, we report directly the corrected functions. However, we report in the inset of the top subfigure of Figure 3 an example of a non-normalized oxygen−oxygen $g(r)$ for the highest and the lowest temperature investigated.

In Figure 3 we can observe that for all the three $g(r)$ at the temperature T_F = 310 K sharp peaks abruptly arise. This temperature is the same where the potential energy behavior shows a drop. The rise of these peaks is proof of the formation of an ordered structure of the water molecules inside the nanotube.

The same phenomenon happens for all the different sizes of the nanotubes. In Figure 4 we show the radial distribution functions $g_{OO}(r)$, $g_{OH}(r)$, and $g_{HH}(r)$ for all temperatures investigated and for all the different sizes of the SWCNT simulated. The abrupt change of structure with the appearance of sharp peaks always happens in correspondence with the temperatures highlighted in the Figure 2 that correspond to the sharp drop of the potential energy. This finding confirms that

DOI: 10.1021/acs.jpcb.7b06306
J. Phys. Chem. B 2017, 121, 10371−10381

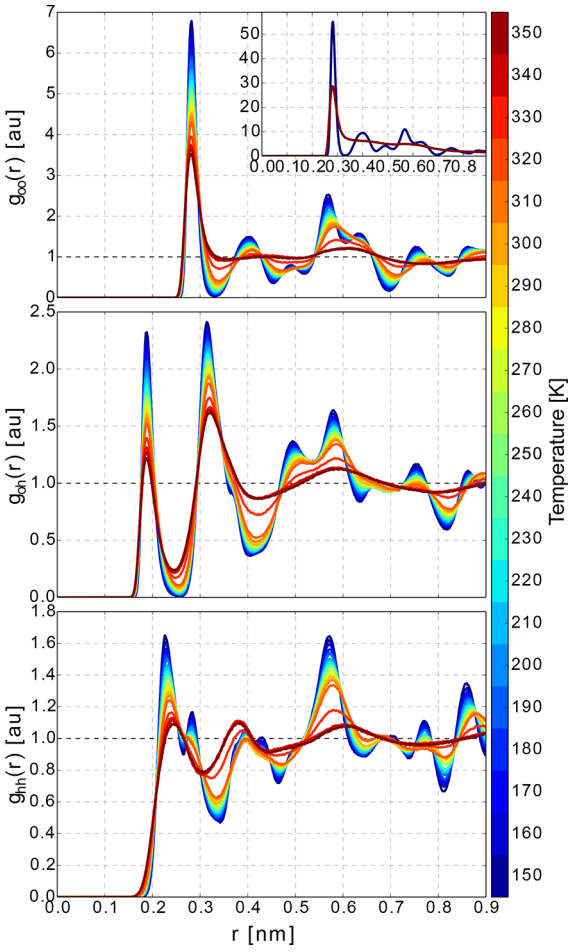

Figure 3. Oxygen−oxygen, oxygen−hydrogen, and hydrogen−hydrogen radial distribution functions for different temperatures for the nanotube with a diameter of 1.291 nm for this system T_F = 310 K. In the subplot of the top figure are reported two $g_{OO}(r)$ without the correction on the normalization relative to the highest temperature (350 K) and the lowest temperature (150 K). In the color maps on the right it is possible to see the relation between the color and the temperature.

those temperatures can be taken as the freezing temperatures of water in the different nanotubes.

The list of all the freezing temperatures as a function of the diameter investigated is reported in Table 4. It is really interesting to note how the freezing temperature increases when the pore becomes smaller, with the exception of the smallest one, d = 0.978 nm, that has a T_F lower than the next larger one. This shows, together with the different qualitative behavior of the potential energy, that there is a crossover in the behavior of the water inside the nanotube around d = 1 nm.

As stated in the Introduction, we used for this simulation an extremely realistic potential for water, the TIP4P/ICE. For this potential the freezing temperature of bulk water is T_F = 270 ± 3 K for P = 1 bar,[25] so only 3.15 K below the experimental value. As can be seen in Table 4, the freezing inside the SWCNT can occur at much higher temperatures with respect to the bulk water, depending on the diameter of the nanotube.

We compare now the results of three freezing temperatures for three different diameters of the SWCNTs just recently measured by the Strano team at MIT[23] with our freezing temperatures and with the results of the freezing temperatures calculated in the pioneering paper by Koga et al.[22] using TIP4P water. We recall here that the freezing point of TIP4P bulk water is T_F = 230.5 ± 3 K,[25] so it is 42.65 K below the experimental water. Agrawal et al.[23] unexpectedly and interestingly found for SWCNTs with diameters of 1.05 and 1.06 nm freezing temperatures close to the boiling temperature of bulk water. In particular the freezing temperature for the 1.05 nm diameter nanotube was higher than the boiling temperature of bulk water.

In Figure 5 we report these data. As we can see, our qualitative trend of the freezing temperatures as a function of the pore diameter is similar to the Koga et al. results. Nonetheless the use of the TIP4P/ICE model gives results in much better quantitative agreement with experiments especially for the d = 1.056 nm SWCNT and succeeds in reproducing the interesting experimental high freezing temperatures. This confirms that the use of a potential that better reproduces the experimental freezing point in bulk water gives results in close agreement with experiments also inside the nanotube.

The lines show a maximum, and for the smallest diameter investigated the freezing temperature goes down showing a change of trend for the smallest pore as already previously noted.

In order to better understand the cooling process inside the nanotube, we report in Figure 6 a scatter plot that describes the distribution of the different atoms inside the nanotube. In the Figure 6 for each nanotube we show four configurations at different temperatures: the highest and the lowest investigated and the two right above and right below the transition temperature. Just below the transition temperature we can see that the system starts to show an angular ordering. In all nanotubes, except the smallest one, it can be seen that the water molecules order forming the ice structure of an ice nanotube. In the right column of the Figure 6 (the one at lowest temperature) we can clearly distinguish the different spots formed by the atoms that constitute the ice ring. We can see that the number of the atoms that form the ice rings goes from 4 to 7. Differently, the smallest nanotube does not show any preferential ordering in the angular coordinate. In order to better understand what is happening in this smaller system, we cannot limit ourselves to observe the projection on the xz plane and we will see later more details on this structure.

In Figure 6 we can observe that the oxygen groups are connected by groups of hydrogens; these hydrogens are the ones that form the hydrogen bond between two water molecules of the same ring. The second hydrogen of the water molecule forms a hydrogen bond with other water molecules belonging to another ring. We do not clearly distinguish them in this plot because these hydrogens form a spot that has the same angular coordinates as the oxygen spots, and they are superimposed in the figure.

Another useful quantity to study the behavior of water upon cooling in the SWCNTs is the radial density distribution ρ:

$$\rho(r) = \frac{N(r + \Delta r)}{2\pi r \Delta r} \tag{3}$$

where $N(r + \Delta r)$ is the number of atoms in the crown of internal radius $r - \Delta r/2$ and external radius $r + \Delta r/2$. The area of the circular crown is the normalization factor $2\pi r\Delta r$.

The $\rho(r)$ data are reported in the Figure 7, in which the distribution for the oxygen and the hydrogen atoms are represented in the filled histogram and the sum of the two distributions is represented in the empty histogram. For each nanotube we show the same temperatures as Figure 6 in order

DOI: 10.1021/acs.jpcb.7b06306
J. Phys. Chem. B 2017, 121, 10371−10381

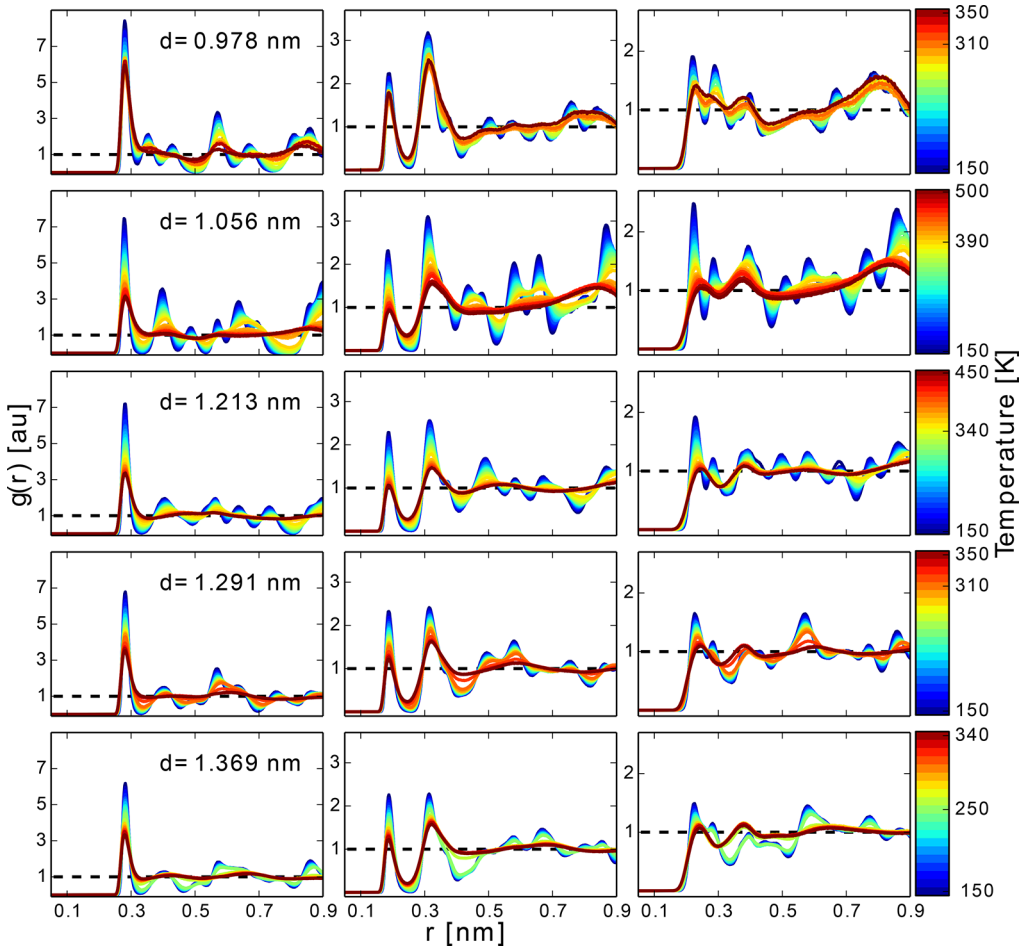

Figure 4. Oxygen−oxygen (left column), oxygen−hydrogen (center column), and hydrogen−hydrogen (right column) radial distribution functions for different temperatures for all the nanotubes investigated spanning from a diameter of 0.978 nm (top row) to a diameter of 1.369 nm (bottom row). In the color maps on the right it is possible to see the relation between the color and the temperature. The temperatures labeled in the color maps are respectively T_{max}, T_F, and T_{min}.

Table 4. Freezing Temperatures (T_F) for the Different Diameters (d) of the Nanotubes

d [nm]	0.978	1.056	1.213	1.291	1.369
T_F [K]	310	390	340	310	250

to compare the two figures. The black vertical line represents the wall of the SWCNT and the shaded region is the space outside.

In Figure 7 we can clearly distinguish for each row in the four panels the two phases of water. If we look at the total radial density distribution, we see that at high temperatures (leftmost panel) the water is in the liquid phase and the very central part of the SWCNTs is more filled by water molecules. We can observe that there is an empty space between water molecules and the SWCNT internal surface. This implies that the accessible space for the water molecules is less than the diameter of the nanotube. At the lowest temperature the crystallization is complete and we see a single peak between the center and the wall of the nanotube. The largest pore still shows some defects, visible also in the projected snapshots of Figure 6, even for the lowest temperature investigated.

In Figure 7 we also report the radial density distribution $\rho(r)$ of the hydrogens and the oxygens separately in order to highlight the relative positions of the atoms. We can observe that in the plot at the lowest temperature T = 150 K there are

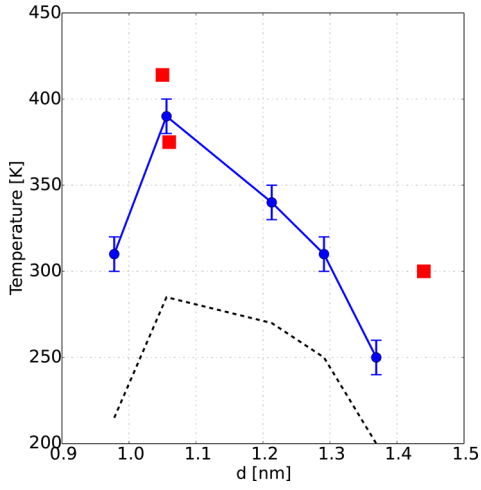

Figure 5. Freezing temperatures of water in SWCNTs obtained from our simulation data using TIP4P/ICE water (filled circles and continuous line), simulation data with TIP4P water reported by Koga et al.[22] (dashed line) and compared with experimental data given by Agrawal et al.[23] (filled squares).

two distinct peaks for the hydrogens distribution. One of these two peaks is closer to the center with respect to the oxygen

DOI: 10.1021/acs.jpcb.7b06306
J. Phys. Chem. B 2017, 121, 10371−10381

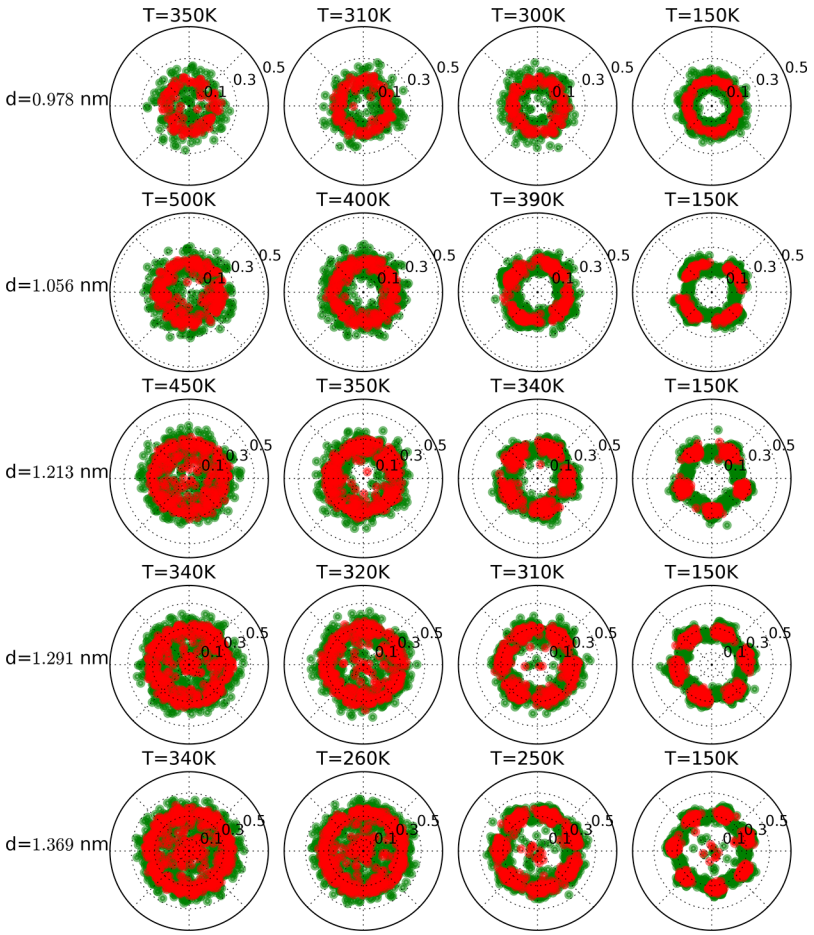

Figure 6. Scatter plot of the different steps in the cooling process for each diameter of SWCNT studied. The red points are the oxygen atoms, and the green ones are the hydrogen atoms. In this plot each point is the projection of the coordinate of atom on the axial plane *xz* that is the transverse plane. In the left column we can see the system at the higher temperature where water is in the liquid phase. In the two central columns we can see the systems just above (center left) and just below (center right) the transition. In the right column we can see the system at the lowest temperature investigated (T = 150 K) that is the same for all the systems.

peak. The other instead is closer to the SWCNT surface. The two peaks are relative to the two hydrogens of the water molecules and represent the radial position of the hydrogen bonds in the ice structure. As we will see better in the last part of this work, the external hydrogens are the ones that form the hydrogen bond between two adjacent rings while the internal ones are related to the intra-ring hydrogen bond.

From Figure 6 and Figure 7 we see that the water molecules show a layering effect due to the SWCNT confinement at high temperatures and for the bigger pores.

Water Ordered Structures inside the SWCNT. In Figure 8 it is possible to see the snapshots of the ice structure crystallized from liquid water in all the nanotubes of different sizes that we have investigated. All the snapshots are taken at the same temperature of T = 150 K that is the lowest temperature that we have simulated.

We can see that water inside nanotubes of diameter larger than 1 nm (from the second to the fifth row) forms an ordered stack of rings when it crystallizes. Upon increasing the diameter of the SWCNT, the water rings become larger passing from rings formed by four molecules up to rings formed by seven molecules. In this Figure 8, it is clearly visualized, similar to what is observed in the Figure 6, that the water molecules that form the rings have two hydrogen bonds, one with a water molecule of the same ring and another one with an oxygen belonging to one of the two adjacent rings. Within the same nanotube in each ring there is always a hydrogen bond between two adjacent molecules, so these hydrogen bonds always point to the adjacent molecule. However, the hydrogen bonds between different rings present disordered orientations.

In the smallest nanotube (d = 0.978 nm) it is not observed the planar ordering of the water molecules that characterizes the structures at larger diameters. The ice structure is formed here by three chains of water molecules twisted together and forming a spiral. This crossover at smaller diameters in the structure of ice is possibly connected to another interesting result. Thomas and McGaughey[11] in their pioneer theoretical work and X. Qin et al.[45] in their experimental work proved in fact that there is a crossover in the flowing behavior of liquid water at exactly the diameter where we observe a crossover in structure, namely, 1 nm.

Our ordered structures are in agreement with those found in the literature on this kind of SWCNT using different model potentials for water; see for example TIP4P,[22] SPC/E.[21] This proves that the results on the structure of the ice nanotubes are very robust, including the crossover in structure type for diameters below 1 nm.

The structure of the ice nanotubes that form inside the SWCNT can be described in a way similar to the description of the SWCNT itself: as a two-dimensional lattice wrapped

DOI: 10.1021/acs.jpcb.7b06306
J. Phys. Chem. B 2017, 121, 10371−10381

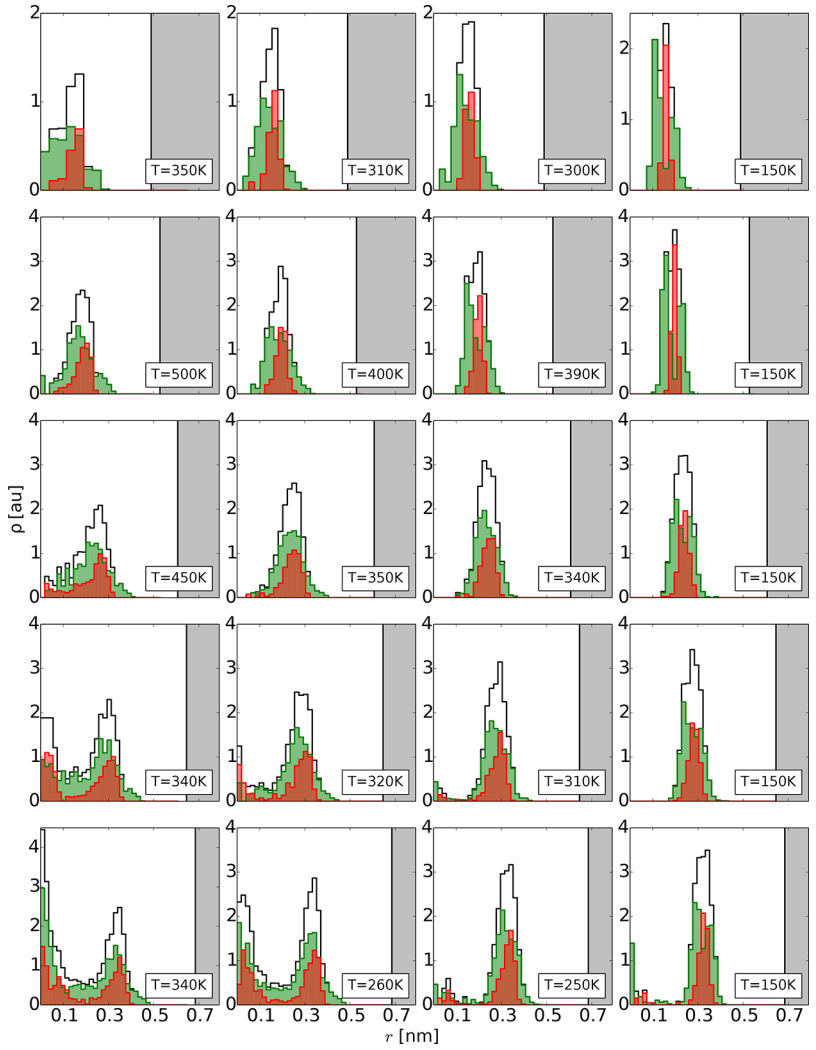

Figure 7. Radial density distribution of the water atoms. The red filled histograms are relative to the distribution of the oxygen atoms, the green filled histograms are relative to the distribution of the hydrogen atoms, and the black empty histograms are relative to the distribution of all the atoms. Each row corresponds to a different diameter of the SWCNT investigated for four selected temperatures: the highest temperature, the closest temperature above freezing, the freezing temperature (T_F), and the lowest temperature. The white regions in the figures are the internal part of the nanotubes.

forming a seamless cylinder.[22] The main difference is that the lattice that would form the ice nanotube is a square lattice instead of the hexagonal lattice formed by the graphene.

In order to better understand the structure of the ice nanotubes, we compare the oxygen−oxygen radial distribution function reported in the Figure 3 with a cartoon of the ice structure obtained for the system with a diameter d = 1.291 nm. This comparison is given by Figure 9. In the cartoon we can see the equilibrium positions of the oxygens. The cartoon was made using the idea of Koga et al.[22] of starting from a square lattice. Assuming that the value of the nearest neighbors distance for two oxygen atoms is defined as l, we can consequently calculate the other distances. The result of the distances calculation for the nearest atoms is reported in Table 5.

Given the value of l, all the other distances are fixed by the geometry of the system. We can obtain the value of the nearest neighbors distance l by the first peak of the oxygen−oxygen $g(r)$. In Figure 9 it be can seen how the peaks in the $g(r)$ are in exact correspondence to the distance reported in Table 5. The second peak in the oxygen−oxygen $g(r)$ is relative to the diagonal of the square lattice that forms the ice nanotube. This gives us a confirmation that the structure of the ice nanotube that we obtained is the one proposed by Koga et al.[22] Moreover, the diagonal is exactly that of a square, and since it coincides with our second peak in the $g(r)$, it means that we have no distortion of the square lattice.

We now concentrate on the position of the hydrogens in the lattice. Observing the behavior of the hydrogen−hydrogen radial distribution function for the lowest temperature shown in the Figure 4, we notice that the second peak is placed in an anomalous position very near the first one. To understand where this peak comes from, we compare in Figure 10 the $g_{OO}(r)$ and the $g_{HH}(r)$ obtained at 150 K for the system with a diameter of the SWCNT d = 1.291 nm. In this figure we can clearly see that the second peak of the $g_{HH}(r)$ is in correspondence with the first peak of the $g_{OO}(r)$. This means that there is a significant number of hydrogens that are at the same relative distance of the two nearest neighbors oxygens. We can conclude that the hydrogens partially mimic the oxygen structure, and this means that there is a partial proton ordering so far never detected in literature.

DOI: 10.1021/acs.jpcb.7b06306
J. Phys. Chem. B 2017, 121, 10371−10381

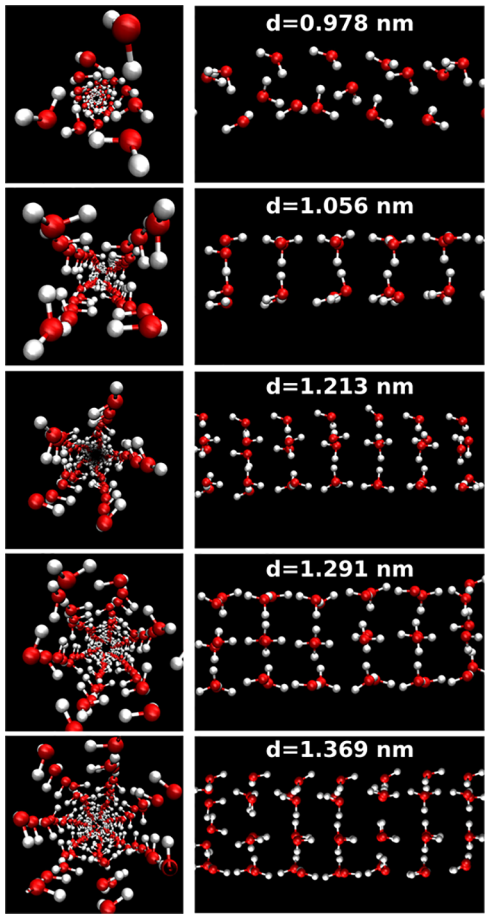

Figure 8. Snapshots of the ice structures obtained inside the SWCNT from our simulation results. All the snapshots are relative to the same temperature at 150 K, and each row corresponds to a different size of the SWCNT. Frontal view (left) and side view (right) are shown.

Finally, in the Figure 11 we report the oxygen−oxygen, oxygen−hydrogen, and hydrogen−hydrogen radial distribution functions for the lowest temperature investigated for all diameter sizes studied. In this figure we highlight with a black dashed line the position of the second peak of the $g_{OO}(r)$. As we previously discussed, the second peak of the $g_{OO}(r)$ is relative to the diagonal of the square lattice. It is interesting to note that the distance where the second peak is located is the same for the structure inside SWCNT with diameters larger than 1 nm. This means that all these ice nanotubes are ideally generated by the same square lattice. Differently, the ice formed in the smallest nanotube has a spiral structure, as previously discussed, leading to a split of the second peak. The first peak remains in the same position, being that the lattice parameter l is not dependent on the nanotube sizes.

In Figure 11 we can also observe that the superposition between the first peak of the $g_{OO}(r)$ and the second peak of the $g_{HH}(r)$ is a feature common to all the systems investigated. We also note that the $g_{OH}(r)$ presents a shoulder in the position situated at distances around l + O−H, where O−H is the constant distance between oxygen and hydrogen within the water molecule in the TIP4P/ICE model. The O−H distances are reported as a black segment in the Figure 11. The shoulder is therefore due to an extra alignment of the water molecules in the different layers of the ice structure, and this strengthens our previous observation on proton ordering.

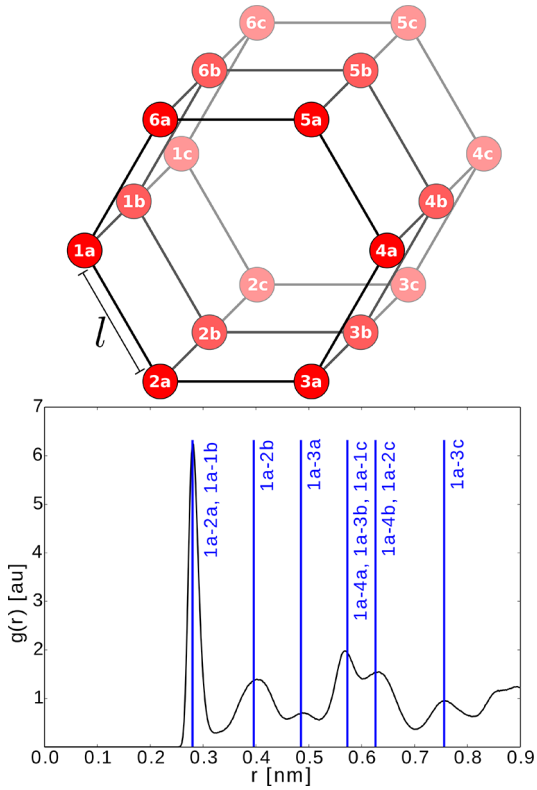

Figure 9. (Top) Cartoon of the oxygen positions in a hexagonal ice nanotube. The distance between the two nearest oxygens is defined by l. This distance is the same for all the oxygens represented. The letters (a, b, c) correspond to the different rings and the numbers (1−6) refer to the position of the oxygens in each ring. (Bottom) $g_{OO}(r)$ as obtained by our simulations at T = 150 K for the d = 1.291 nm SWCNT. The blue vertical lines correspond to the oxygen−oxygen distances reported in the Table 5. Numbers and letters for each vertical line correspond to the distances in the lattice indicated in the top panel.

Table 5. Value of the Distance between Two Different Oxygen in the Structure of Hexagonal Ice Nanotube[a]

distance	value
1a−2a	l
1a−2b	$\sqrt{2}l$
1a−3a	$\sqrt{3}l$
1a−4a, 1a−3b, 1a−1c	$2l$
1a−4b, 1a−2c	$\sqrt{5}l$
1a−3c	$\sqrt{7}l$

[a]The labels of the positions are relative to the cartoon in Figure 9.

To better visualize the proton ordering in the structures that we found in our systems, we report them in Figure 12. In the upper panel we report a general configuration in which the O−O distance is the same as the H−H distance while the intermolecular O−H distance depends on the angle. We know that there are a lot of molecules in which the H−H distance is the same as the O−O distance because of the clear second peak that we observe at that distance on the $g_{HH}(r)$; see Figure 10. These molecules are also visible in the snapshots; see Figure 8.

In the bottom panel we report the configuration that causes the previously observed shoulder in the O−H distribution, see Figure 11, at distances l + O−H. The presence of a shoulder

DOI: 10.1021/acs.jpcb.7b06306
J. Phys. Chem. B 2017, 121, 10371−10381

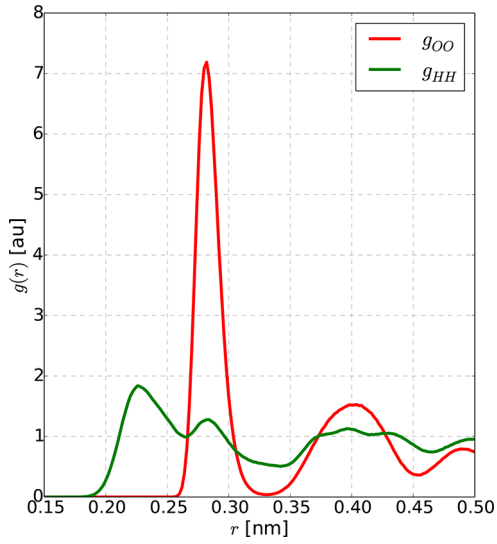

Figure 10. A blowup of the comparison of the $g_{OO}(r)$ and the $g_{HH}(r)$ relative to the SWCTN with diameter of 1.291 nm at 150 K.

means that there is a significant number of water molecules aligned as shown in this second panel.

DISCUSSION AND CONCLUSIONS

In this work we performed molecular dynamics simulations to study the liquid/solid transition of water in carbon nanotubes and to investigate the formation of ice. To describe the water molecules at best, we choose one of the potentials that better reproduces the freezing processes in bulk water: the TIP4P/ICE.[26]

The first issue that we faced was the location of the freezing temperatures T_F for the different sizes of nanotubes investigated. In order to identify the temperatures at which water freezes, we analyzed the behavior of the potential energy. We identify T_F as the temperature where the potential energy shows an abrupt decrease. To support this analysis, we analyzed also the behavior of the water radial distribution function $g_{ij}(r)$. The $g_{ij}(r)$ show a sudden change exactly in correspondence of the freezing temperature predicted with the potential energy behavior, confirming the location of the freezing temperatures. In the five different pores that we investigated, we observed a maximum value of T_F for the SWCNT of diameter d = 1.056 nm.

Importantly, with the potential model that we used, we obtained freezing temperatures in very good agreement with a recent experiment[23] that discovered for the first time that in these nanotubes water freezes when it boils in the bulk. As the authors declared, the remarkable effect of the enhancement of the freezing temperature of water inside carbon nanotubes is much more consistent than what was expected. We recall here that for the potential that we use, TIP4P/ICE, in the bulk phase the freezing point coincides with the freezing point of experimental water.

In the different nanotubes that we simulated the ordered structures that we find below T_F are different. In particular we observed that for the SWCNT with diameter d = 0.978 nm the water molecules form three chains wrapped together to form a spiral. For all the nanotubes with diameter larger than 1 nm the water forms an ordered stack of rings. When the size of the nanotube grows, the water rings became larger passing from

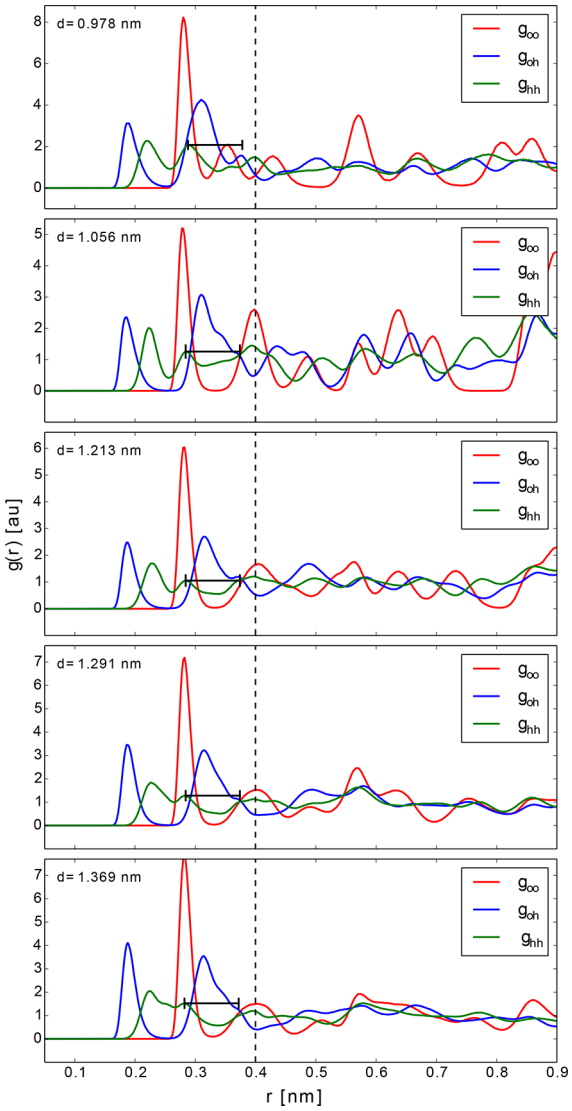

Figure 11. Radial distribution functions for all the nanotubes at the lowest temperature investigated (T = 150 K). Rows correspond to different diameters and columns, from the left, to oxygen−oxygen, oxygen−hydrogen, and hydrogen−hydrogen $g(r)$. The vertical black dashed line marks the peak of the oxygen−oxygen $g(r)$ corresponding to the diagonal of the squares of the lattice. The horizontal black line represent the O−H distance in the TIP4P/ICE model.

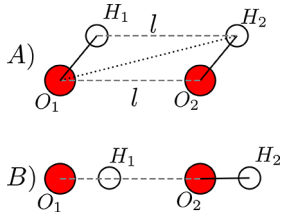

Figure 12. Proton ordering inside carbon nanotubes. The two configurations found in the simulations are reported in panels A and B.

rings formed by four molecules up to rings formed by seven molecules.

These structures are in agreement with those found on this kind of SWCNT using different model potentials for water.[21,22] This proves that the simulation results on the structure of the ice nanotubes are very robust.

DOI: 10.1021/acs.jpcb.7b06306
J. Phys. Chem. B 2017, 121, 10371−10381

In order to deepen and extend our knowledge of the ice nanotubes structure, we made an analysis of the oxygen−oxygen radial distribution function for the system with a diameter of the SWCNT of 1.291 nm. With this analysis we were able to assign the peaks in the $g_{OO}(r)$ to the distances between atoms in the structures and to observe the common features of the different structures obtained in the different pores.

As a novel result, we found the presence of a partial proton ordering in the ice nanotube at finite temperature. The ordering effect is due to the fact that in the ice nanotubes the hydrogens mirror the structure of the oxygens. This produces an anomalous peak in the g_{HH} adjacent to the first peak, and it produces also a shoulder in the g_{OH}.

In conclusions, given our results, TIP4P/ICE has proven to be an excellent potential for studying water in SWCNT.

AUTHOR INFORMATION

Corresponding Author

*E-mail: gallop@fis.uniroma3.it.

ORCID

P. Gallo: 0000-0003-4370-9071

Notes

The authors declare no competing financial interest.

REFERENCES

(1) Gallo, P.; Amann-Winkel, K.; Angell, C. A.; Anisimov, M. A.; Caupin, F.; Chakravarty, C.; Lascaris, E.; Loerting, T.; Panagiotopoulos, A. Z.; Russo, J.; et al. Water: A Tale of Two Liquids. *Chem. Rev.* **2016**, *116*, 7463−7500 (PMID: 27380438).

(2) Franks, F. *Water: A Matrix of Life*; RSC Paperbacks; The Royal Society of Chemistry: Cambridge, U.K., 2007.

(3) Liu, L.; Chen, S.-H.; Faraone, A.; Yen, C.-W.; Mou, C.-Y. Pressure Dependence of Fragile-to-Strong Transition and a Possible Second Critical Point in Supercooled Confined Water. *Phys. Rev. Lett.* **2005**, *95*, 117802.

(4) Gallo, P.; Rovere, M.; Chen, S.-H. Dynamic Crossover in Supercooled Confined Water: Understanding Bulk Properties through Confinement. *J. Phys. Chem. Lett.* **2010**, *1*, 729−733.

(5) Rasaiah, J. C.; Garde, S.; Hummer, G. Water in Nonpolar Confinement: From Nanotubes to Proteins and Beyond. *Annu. Rev. Phys. Chem.* **2008**, *59*, 713−740 (PMID: 18092942).

(6) De Volder, M. F. L.; Tawfick, S. H.; Baughman, R. H.; Hart, A. J. Carbon Nanotubes: Present and Future Commercial Applications. *Science* **2013**, *339*, 535−539.

(7) Hierold, C.; Jungen, A.; Stampfer, C.; Helbling, T. Nano Electromechanical Sensors Based on Carbon Nanotubes. *Sens. Actuators, A* **2007**, *136*, 51−61 (25th Anniversary of *Sensors and Actuators A: Physical*).

(8) Liu, Z.; Tabakman, S.; Welsher, K.; Dai, H. Carbon Nanotubes in Biology And Medicine: in Vitro and in Vivo Detection, Imaging and Drug Delivery. *Nano Res.* **2009**, *2*, 85−120.

(9) Zanello, L. P.; Zhao, B.; Hu, H.; Haddon, R. C. Bone Cell Proliferation on Carbon Nanotubes. *Nano Lett.* **2006**, *6*, 562−567.

(10) Bordin, J. R.; Barbosa, M. C. Flow and Structure of Fluids in Functionalized Nanopores. *Phys. A* **2017**, *467*, 137−147.

(11) Thomas, J. A.; McGaughey, A. J. H. Water Flow in Carbon Nanotubes: Transition to Subcontinuum Transport. *Phys. Rev. Lett.* **2009**, *102*, 184502.

(12) Majumder, M.; Chopra, N.; Andrews, R.; Hinds, B. J. Nanoscale Hydrodynamics: Enhanced Flow in Carbon Nanotubes. *Nature* **2005**, *438*, 44−44.

(13) Cohen-Tanugi, D.; Grossman, J. C. Water Desalination across Nanoporous Graphene. *Nano Lett.* **2012**, *12*, 3602−3608 (PMID: 22668008).

(14) Corry, B. Designing Carbon Nanotube Membranes for Efficient Water Desalination. *J. Phys. Chem. B* **2008**, *112*, 1427−1434 (PMID: 18163610).

(15) Maniwa, Y.; Kataura, H.; Abe, M.; Suzuki, S.; Achiba, Y.; Kira, H.; Matsuda, K. Phase Transition in Confined Water Inside Carbon Nanotubes. *J. Phys. Soc. Jpn.* **2002**, *71*, 2863−2866.

(16) Maniwa, Y.; Kataura, H.; Abe, M.; Udaka, A.; Suzuki, S.; Achiba, Y.; Kira, H.; Matsuda, K.; Kadowaki, H.; Okabe, Y. Ordered Water Inside Carbon Nanotubes: Formation of Pentagonal to Octagonal Ice-Nanotubes. *Chem. Phys. Lett.* **2005**, *401*, 534−538.

(17) Ghosh, S.; Ramanathan, K. V.; Sood, A. K. Water at Nanoscale Confined In Single-Walled Carbon Nanotubes Studied by NMR. *Europhys. Lett.* **2004**, *65*, 678.

(18) Kolesnikov, A. I.; Zanotti, J.-M.; Loong, C.-K.; Thiyagarajan, P.; Moravsky, A. P.; Loutfy, R. O.; Burnham, C. J. Anomalously Soft Dynamics of Water in a Nanotube: A Revelation of Nanoscale Confinement. *Phys. Rev. Lett.* **2004**, *93*, 035503.

(19) Byl, O.; Liu, J.-C.; Wang, Y.; Yim, W.-L.; Johnson, J. K.; Yates, J. T. Unusual Hydrogen Bonding in Water-Filled Carbon Nanotubes. *J. Am. Chem. Soc.* **2006**, *128*, 12090−12097 (PMID: 16967958).

(20) Takaiwa, D.; Hatano, I.; Koga, K.; Tanaka, H. Phase Diagram of Water in Carbon Nanotubes. *Proc. Natl. Acad. Sci. U. S. A.* **2008**, *105*, 39−43.

(21) Shiomi, J.; Kimura, T.; Maruyama, S. Molecular Dynamics of Ice-Nanotube Formation Inside Carbon Nanotubes. *J. Phys. Chem. C* **2007**, *111*, 12188−12193.

(22) Koga, K.; Parra, R. D.; Tanaka, H.; Zeng, X. C. Ice Nanotube: What Does he Unit Cell Look Like? *J. Chem. Phys.* **2000**, *113*, 5037−5040.

(23) Agrawal, K. V.; Shimizu, S.; Drahushuk, L. W.; Kilcoyne, D.; Strano, M. S. Observation of Extreme Phase Transition Temperatures of Water Confined inside Isolated Carbon Nanotubes. *Nat. Nanotechnol.* **2017**, *12*, 267−273.

(24) Cabeza, L.; Mehling, H.; Hiebler, S.; Ziegler, F. Heat Transfer Enhancement in Water When Used a {PCM} in Thermal Energy Storage. *Appl. Therm. Eng.* **2002**, *22*, 1141−1151.

(25) Fernández, R. G.; Abascal, J. L. F.; Vega, C. The Melting Point of Ice Ih for Common Water Models Calculated from Direct Coexistence of the Solid-Liquid Interface. *J. Chem. Phys.* **2006**, *124*, 144506.

(26) Abascal, J. L. F.; Sanz, E.; Fernández, R. G.; Vega, C. A Potential Model for the Study of Ices and Amorphous Water: TIP4P/Ice. *J. Chem. Phys.* **2005**, *122*, 234511.

(27) Haji-Akbari, A.; Debenedetti, P. G. Computational Investigation of Surface Freezing in a Molecular Model of Water. *Proc. Natl. Acad. Sci. U. S. A.* **2017**, *114*, 3316−3321.

(28) Geng, H.; Liu, X.; Shi, G.; Bai, G.; Ma, J.; Chen, J.; Wu, Z.; Song, Y.; Fang, H.; Wang, J. Graphene Oxide Restricts Growth and Recrystallization of Ice Crystals. *Angew. Chem., Int. Ed.* **2017**, *56*, 997−1001.

(29) Espinosa, J. R.; Navarro, C.; Sanz, E.; Valeriani, C.; Vega, C. On the Time Required to Freeze Water. *J. Chem. Phys.* **2016**, *145*, 211922.

(30) Conde, M. M.; Vega, C.; Patrykiejew, A. The Thickness of a Liquid Layer on the Free Surface of Ice as Obtained from Computer Simulation. *J. Chem. Phys.* **2008**, *129*, 014702.

(31) Vega, C.; de Miguel, E. Surface Tension of the Most Popular Models of Water by using the Test-Area Simulation Method. *J. Chem. Phys.* **2007**, *126*, 154707.

(32) Vega, C.; Abascal, J. L. F.; Nezbeda, I. Vapor-Liquid Equilibria from the Triple Point up to the Critical Point for the New Generation of TIP4P-Like Models: TIP4P/Ew, TIP4P/2005, and TIP4P/ice. *J. Chem. Phys.* **2006**, *125*, 034503.

(33) Martin-Conde, M.; MacDowell, L. G.; Vega, C. Computer Simulation of Two New Solid Phases of water: Ice XIII and ice XIV. *J. Chem. Phys.* **2006**, *125*, 116101.

(34) Míguez, J. M.; Conde, M. M.; Torré, J.-P.; Blas, F. J.; Piñeiro, M. M.; Vega, C. Molecular Dynamics Simulation of CO2 Hydrates: Prediction of Three Phase Coexistence Line. *J. Chem. Phys.* **2015**, *142*, 124505.

DOI: 10.1021/acs.jpcb.7b06306
J. Phys. Chem. B 2017, 121, 10371−10381

(35) Conde, M. M.; Vega, C. Determining the Three-Phase Coexistence Line in Methane Hydrates using Computer Simulations. *J. Chem. Phys.* **2010**, *133*, 064507.
(36) Bagherzadeh, S. A.; Alavi, S.; Ripmeester, J. A.; Englezos, P. Evolution of Methane During Gas Hydrate Dissociation. *Fluid Phase Equilib.* **2013**, *358*, 114−120.
(37) Walsh, M. R.; Koh, C. A.; Sloan, E. D.; Sum, A. K.; Wu, D. T. Microsecond Simulations of Spontaneous Methane Hydrate Nucleation and Growth. *Science* **2009**, *326*, 1095−1098.
(38) Narita, N.; Nagai, S.; Suzuki, S.; Nakao, K. Optimized Geometries and Electronic Structures of Graphyne and its Family. *Phys. Rev. B: Condens. Matter Mater. Phys.* **1998**, *58*, 11009−11014.
(39) Gupta, A. K.; Russin, T. J.; Gutiérrez, H. R.; Eklund, P. C. Probing Graphene Edges via Raman Scattering. *ACS Nano* **2009**, *3*, 45−52.
(40) Kaminski, G. A.; Friesner, R. A.; Tirado-Rives, J.; Jorgensen, W. L. Evaluation and Reparametrization of the OPLS-AA Force Field for Proteins via Comparison with Accurate Quantum Chemical Calculations on Peptides. *J. Phys. Chem. B* **2001**, *105*, 6474−6487.
(41) Abraham, M. J.; Murtola, T.; Schulz, R.; Páll, S.; Smith, J. C.; Hess, B.; Lindahl, E. GROMACS: High Performance Molecular Simulations Through Multi-Level Parallelism from Laptops to Supercomputers. *SoftwareX* **2015**, *1−2*, 19−25.
(42) Best, R. B.; Hummer, G. Reaction Coordinates and Rates from Transition Paths. *Proc. Natl. Acad. Sci. U. S. A.* **2005**, *102*, 6732−6737.
(43) De Marzio, M.; Camisasca, G.; Conde, M. M.; Rovere, M.; Gallo, P. Structural Properties and Fragile to Strong Transition in Confined Water. *J. Chem. Phys.* **2017**, *146*, 084505.
(44) Gallo, P.; Ricci, M. A.; Rovere, M. Layer Analysis of The Structure of Water Confined in Vycor Glass. *J. Chem. Phys.* **2002**, *116*, 342−346.
(45) Qin, X.; Yuan, Q.; Zhao, Y.; Xie, S.; Liu, Z. Measurement of the Rate of Water Translocation through Carbon Nanotubes. *Nano Lett.* **2011**, *11*, 2173−2177 (PMID: 21462938).

DOI: 10.1021/acs.jpcb.7b06306
J. Phys. Chem. B 2017, 121, 10371−10381